

Probing sterile neutrinos in the framework of inverse seesaw mechanism through leptoquark productions

Debottam Das,^{*} Kirtiman Ghosh,[†] and Manimala Mitra[‡]

*Institute of Physics, Bhubaneswar 751005,
India & Homi Bhabha National Institute,
Training School Complex, Anushakti Nagar, Mumbai 400085, India*

Subhadeep Mondal[§]

*Regional Centre for Accelerator-based Particle Physics,
Harish-Chandra Research Institute, HBNI, Chhatnag Road,
Jhansi, Allahabad 211019, India & Department of Physics,
and Helsinki Institute of Physics, P. O. Box 64,
FI-00014 University of Helsinki, Finland*

Abstract

We consider an extension of the Standard Model (SM) augmented by two neutral singlet fermions per generation and a leptoquark. In order to generate the light neutrino masses and mixing, we incorporate inverse seesaw mechanism. The right handed neutrino production in this model is significantly larger than the conventional inverse seesaw scenario. We analyze the different collider signatures of this model and find that the final states associated with three or more leptons, multi jet and at least one b-tagged and (or) τ -tagged jet can probe larger RH neutrino mass scale. We have also proposed a same-sign dilepton signal region associated with multiple jets and missing energy that can be used to distinguish the the present scenario from the usual inverse seesaw extended SM.

* debottam@iopb.res.in

† kirti.gh@gmail.com

‡ manimala@iopb.res.in

§ subhadeepmondal@hri.res.in

I. INTRODUCTION

ATLAS and CMS collaborations have already made huge impacts to unravel any possible signatures of physics beyond the Standard Model (BSM) at the LHC [1, 2]. Although no signature of new particles has yet been found by the direct search, there are many reasons for pursuing our search in BSM physics at the LHC. Undoubtedly, one of the most compelling motivations comes from the existence of non-zero neutrino masses and substantial mixing among the three light neutrino states (see for example, [3, 4]). In this frontier, the neutrino oscillation experiments have made significant progress to measure the mass square difference and the mixing angles of the neutrinos with unprecedented precision, which indicates that at least two of the light neutrino states have to have tiny non-zero masses. As a natural consequence, many proposals have been put forward over the years to accommodate the neutrino masses and mixing in the theory of which various *Seesaw Mechanisms* have remained of primary interest [5–16].

The simplest seesaw extension, known as the *Type-I Seesaw mechanism* [5–8] is accompanied with additional Majorana right-handed neutrinos (ν_{Ri}). Light neutrinos gain tiny non-zero masses by virtue of their mixings with these heavy neutrino states. In such scenarios, the mass scale of these Majorana neutrinos has to lie very close to gauge coupling unification scale $M_G \sim 10^{16}$ GeV in order to account for the tiny neutrino masses. Such a massive ν_R completely decouples from the low energy theory and remains out of the kinematic reach of the LHC. One can of course bring down this mass scale to TeV range, but at the cost of a very small Dirac neutrino Yukawa coupling ($\sim 10^{-6}$) which again makes any possible phenomenological aspects of the heavy neutrinos unforeseeable at the LHC¹. Thus the lack of predictability of this simplistic scenario has forced theorists as well as experimentalists to study models which can readily be probed at the LHC with the existing data. One such scenario is called the *inverse seesaw* mechanism [18–20] where the SM particle content is augmented by two singlet neutrinos with opposite lepton numbers (+1 and -1). The generic form of the light neutrino mass can be expressed as $m_\nu \sim (m_D^2/M_R^2)\mu$, where $m_D \sim Y_\nu v$ represents the Dirac neutrino mass term, v , the electroweak VEV, Y_ν , a generic Yukawa coupling and μ , a lepton number violating ($\Delta L = 2$) mass parameter which can be kept naturally small [21]. The presence of this small (\sim eV) $\Delta L = 2$ mass term helps to keep

¹ Such small couplings can only be probed with very high precision colliders and naturally lepton colliders are better suited to serve the purpose [17].

the sterile neutrino mass scale M_R close to TeV, i.e., within the reach of LHC, with order one Yukawa coupling. This feature of the model leads to a plethora of testable phenomenological consequences [22–32] which have been studied quite extensively in the context of present and future collider experiments [33–42]. For the RH neutrino production through vector boson fusion and higher order corrections, see [43, 44]. Note that, although the heavy neutrino states now lie within the kinematic reach of the LHC, the production processes are still driven by the charged/neutral current weak interactions, through active-sterile neutrino mixing, that depend crucially on the mass scale of the RH neutrinos M_R . Hence, the cross-section falls rapidly with increasing heavy neutrino masses and with smaller mixings. The production cross-section of the RH neutrinos can be drastically enhanced in presence of leptoquarks (LQ). Leptoquarks, being charged under $SU(3)_C$, are copiously produced at the LHC. The right-handed neutrinos can result from the decays of LQs. It is important to note that in this case, the RH neutrino production does not depend on the active-sterile mixing. Therefore, RH neutrinos can be probed at the LHC irrespective of their mixing with the active component as long as they decay inside the detector.

Introduction of LQ (for a recent review see [45]) to the SM Lagrangian is motivated from a quite different viewpoint. In fact, in the Pati-Salam model that LQs are a natural outcome of unification of quarks and leptons [46]. The presence of these new exotic particles has been further motivated by the simple grand unified gauge groups of $SU(5)$ [47] and $SO(10)$ [48, 49]. While both vector (spin-one) and scalar LQ (spin-zero) states are possible in local quantum field theories, the scalar states are more attractive as they do not lead to any potential problems related to loop corrections [50, 51]. Moreover, it has recently been shown that the scalar LQs are indeed very useful to explain various B -physics anomalies like R_K [52] or R_{D^*} [53]. Explanation of both R_K and R_D anomalies with a scalar LQ with the hypercharge $Y = \frac{1}{6}$ would be possible if one includes a new interaction between a scalar LQ and a right handed neutrino [51]. Keeping in mind that the presence of a LQ- ν_R coupling is highly motivated to accommodate B -physics anomalies, in this work we will go one step further. We will introduce additional sterile neutrinos in the model to comply with all existing experimental data on light neutrino mass and mixing angles while the mass of the heavy neutrino states have been kept smaller than the leptoquark states. In practice, we incorporate *inverse seesaw* to the SM extended by leptoquarks for our study. We show that the heavy neutrinos can be copiously generated from the decays of the scalar LQs which

can be produced via strong interactions thanks to their $SU(3)$ interactions. The relevant couplings and masses of the LQs and the heavy neutrinos are chosen in a way such that they are consistent with the experimental constraints and at the same time maximize the heavy neutrino productions from the cascade decay. Moreover our collider study shows that such a scenario has the potential of probing heavy neutrino masses up to a much higher range compared to that in the usual neutrino mass models.

The paper is organized as follows. In Sec. II, we introduce the model. Following that, in Section. III, we discuss the present experimental constraints on the RH neutrinos and the LQs. The collider signatures have been discussed in Section. IV. Finally, we present our conclusion.

II. INVERSE SEESAW MECHANISM IN THE SM EXTENDED BY LEPTO-QUARKS

The Lagrangian which we will consider in this work can be cast as

$$\mathcal{L} = \mathcal{L}_{SM} + \mathcal{L}_{\Delta} + \mathcal{L}_{IS} . \quad (1)$$

\mathcal{L}_{Δ} includes the interaction terms between the leptoquarks and the SM particles while \mathcal{L}_{IS} comprises of the relevant terms for generation of the neutrino mass and mixing angles. The association between Δ and \mathcal{L}_{IS} have been realized through right handed neutrino states ν_{Ri} whose mass can vary $\mathcal{O}(1) \text{ eV} \leq M_{Ri} \leq \mathcal{O}(1) \text{ TeV}$. Moreover the inverse seesaw extension of the SM requires three new fermionic singlet fields X_i ($i = 1, 2, 3$) with lepton numbers $+1$ in contrast to the ν_{Ri} states of lepton numbers -1 respectively².

$$\mathcal{L} \in \varepsilon_{ab} Y_{\nu}^{ij} \nu_i^R L_j^a H^b + M_{Ri} \nu_{Ri} X_i + \frac{1}{2} \mu_{X_{ij}} X_i X_j , \quad (2)$$

where $i, j = 1, 2, 3$ denote generation indices. In the above L_i denotes three generation $SU(2)$ lepton doublets. M_{Ri} represents the right-handed neutrino bilinear term which conserves lepton number. The total lepton number L is no longer a good quantum number because of non-vanishing μ_X , though $(-1)^L$ is still a good symmetry. Clearly, as $\mu_{X_i} \rightarrow 0$, lepton number conservation is restored, since M_R does not violate lepton number.

² Note that in the minimal inverse seesaw extension of the SM, two pairs of the singlet field would be sufficient to satisfy all neutrino data [54].

The Leptoquark part of the Lagrangian for a scalar LQ state Δ transforms as $\Delta \in (3, 2, \frac{1}{6})$ under the SM gauge group can be written as [45, 51]

$$\mathcal{L}_\Delta = \bar{d}_R Y_L (\tilde{\Delta})^\dagger L + \bar{Q} Y_R \Delta \nu_R + \text{h.c.}; \quad (3)$$

where $\tilde{\Delta} = i\sigma_2 \Delta^*$. Defining mass eigenstates for a fermionic field $\psi_{L,R}^i$ as $\psi_{L,R}^{mi} = U_{L,R}^i \psi_{L,R}^i$ [51], one can get (for simplicity we remove the superscript m from the fields in mass basis.)

$$\begin{aligned} \mathcal{L}_\Delta = & Y_L^{ij} \bar{d}_R^i U_{\text{PMNS}}^{jk} \nu_L^k \Delta^{(-1/3)} - Y_L^{ij} \bar{d}_R^i \ell_L^j \Delta^{(2/3)} \\ & + Y_R^{ij} \bar{u}_L^i \nu_R^j \Delta^{(2/3)} + Y_R^{ij} \bar{d}_L^i V_{\text{CKM}}^{kj} \nu_R^k \Delta^{(-1/3)} + \text{h.c.}, \end{aligned} \quad (4)$$

where $Y_L \rightarrow U_R^{d\dagger} Y_L U_L^\ell$ and $Y_R \rightarrow U_L^{u\dagger} Y_R U_R^\nu$ have been used. Similarly, $U_{\text{PMNS}} = U_L^\ell U_L^{\nu\dagger}$, and $V_{\text{CKM}} = U_L^d U_L^{u\dagger}$ represent the Pontecorvo-Maki-Nakagawa-Sakata and the Cabibbo-Kobayashi-Maskawa matrices. Now assuming the Yukawa couplings to the first generations of the quarks/leptons as zero to become consistent with the atomic parity violation experiments [45], we represent the matrices as follows [51]:

$$Y_{L,R} = \begin{pmatrix} 0 & 0 & 0 \\ 0 & Y_{L,R}^{22} & Y_{L,R}^{23} \\ 0 & Y_{L,R}^{32} & Y_{L,R}^{33} \end{pmatrix}.$$

Here we primarily consider productions of $\Delta^{(2/3)}$ states because of its direct coupling with t quarks and the third generation RH neutrinos ν_{R_3} . In the following we consider two scenarios. (i) Yukawa couplings that can potentially explain the B -physics anomalies. Here $Y_{L,R}^{2i}$ can be small, while $Y_{L,R}^{3i}$ can be large. In particular there is a lower bound on $Y_L^{33} \geq 1.5$ [55] which we will use for our calculation (ii) Yukawa couplings of the 2nd and 3rd generations are unconstrained from B -physics, though the choice of Y_R^{33} is completely driven by the fact that we need to maximize the branching ratio $\text{LQ} \rightarrow tN_\tau$.

A. Neutrino masses in Inverse seesaw

We consider a general framework with three generations for the sterile neutrinos, namely ν_{Ri} and X_i . Consequently, one has the following symmetric (9×9) mass matrix \mathcal{M} in the

basis $\{\nu, \nu_R, X\}$,

$$\mathcal{M} = \begin{pmatrix} 0 & m_D^T & 0 \\ m_D & 0 & M_R \\ 0 & M_R^T & \mu_X \end{pmatrix}, \quad (5)$$

Where, $m_D = \frac{1}{\sqrt{2}}Y_\nu v$ and M_R, μ_X are (3×3) matrices in family space. Assuming $(m_D, \mu_X \ll M_R)$ the diagonalisation results in an effective Majorana mass matrix for the light neutrinos

$$m_\nu = m_D^T M_R^{T-1} \mu_X M_R^{-1} m_D = \frac{v^2}{2} Y_\nu^T (M_R^T)^{-1} \mu_X M_R^{-1} Y_\nu. \quad (6)$$

The most important aspect of the inverse seesaw mechanism is that the smallness of the light neutrino masses is directly controlled by the scale of μ_X . Having this small dimensionful term in the Lagrangian is technically natural in the sense of 't Hooft [21], as in the limit of vanishing μ_X one recovers the lepton number symmetry. The lepton number conserving mass parameters m_D and M_R can easily accommodate large (natural) Yukawa couplings ($Y_\nu \sim \mathcal{O}(1)$) and a right-handed neutrino mass scale around the TeV, see Eq. (6). In analogy to a type-I seesaw, one can define an effective right-handed neutrino mass term M such that

$$M^{-1} = (M_R^T)^{-1} \cdot \mu_X \cdot M_R^{-1}. \quad (7)$$

With this definition, the light neutrino mass matrix can be cast in a way which strongly resembles a standard (type-I) seesaw equation

$$m_\nu = \frac{v^2}{2} Y_\nu^T M^{-1} Y_\nu. \quad (8)$$

This effective light neutrino mass matrix (m_ν) can be diagonalized as

$$U_{PMNS}^T m_\nu U_{PMNS} = \text{diag } m_i. \quad (9)$$

In the subsequent analysis, we assume M_R and Y_ν are diagonal ($M_{R_{ij}} = \text{diag } M_{R_{ii}}, Y_{\nu_{ij}} = \text{diag } Y_{\nu_{ii}}$). This choice of $\text{diag } Y_{\nu_{ii}}$ naturally ameliorates constraints from lepton flavor changing processes. However, $\mu_{X_{ij}}$ is not flavor diagonal and its structure can be determined by using Eq. 7, Eq. 8, and Eq. 9 where the present results on neutrino data [4] have been used.

In our analysis, we have used the best-fit values of the mass square differences and the mixing angles to fit μ_X . The light neutrino masses and the PMNS mixing matrix have been depicted in Tab. 1.

Parameters	Values
$\sin^2\theta_{12}$	$0.304^{+0.013}_{-0.012}$
$\sin^2\theta_{23}$	$0.452^{+0.052}_{-0.028}$
$\sin^2\theta_{13}$	$0.0218^{+0.001}_{-0.001}$
$\Delta m_{21}^2 \text{ eV}^2$	$(7.50^{+0.19}_{-0.17}) \times 10^{-5}$
$\Delta m_{32}^2 \text{ eV}^2$	$(2.457^{+0.047}_{-0.047}) \times 10^{-3}$
PMNS [4]	$\begin{pmatrix} 0.801 - 0.845 & 0.225 - 0.517 & 0.246 - 0.529 \\ 0.514 - 0.580 & 0.441 - 0.699 & 0.464 - 0.713 \\ 0.137 - 0.158 & 0.614 - 0.793 & 0.590 - 0.776 \end{pmatrix}$

TABLE 1. Three flavor neutrino oscillation data obtained from global fit for normal hierarchy in neutrino masses and the PMNS matrix elements with their 3σ allowed ranges. We have only used the best-fit values of the mass square differences and the mixing angles to fit an off-diagonal μ_X in order to fit the neutrino oscillation data.

B. Production and decay of Leptoquarks

Being triplet under $SU(3)_C$, leptoquarks have gauge couplings with gluons. Therefore, at the LHC, leptoquarks are produced in pairs via gluon-gluon and quark-antiquark initiated processes. Gluon-gluon initiated processes primarily proceed through a leptoquark exchange in the $t(u)$ -channel or a gluon exchange in the s -channel. On the other hand, quark-antiquark initiated processes take place only via a gluon exchange in the s -channel and hence, suppressed compared to the $t(u)$ -channel leptoquark exchange. Leptoquark can also couple to a quark-lepton pair via Yukawa interactions as shown in Eq. 4. Therefore, quark-antiquark initiated processes may also proceed through a lepton (charged or neutral) exchange in the $t(u)$ -channel. However, the Yukawa couplings of the leptoquarks with the first generation of quarks and leptons are severely constrained from the atomic parity violation experiments [45], making this contribution small. In order to generate the model files for further simulation, we have incorporated the new physics Lagrangian in FeynRules (v2.3.13) [56, 57] and subsequently generated model files are used to compute particle spectrum, relevant branching ratios and cross-sections via MadGraph5 (v2.4.3) [58, 59] with NNPDF23lo1 [60, 61] parton distribution function (PDF). We have used dynamic definition [62] of the factorization scale for the PDF and renormalization scale for evaluating the QCD

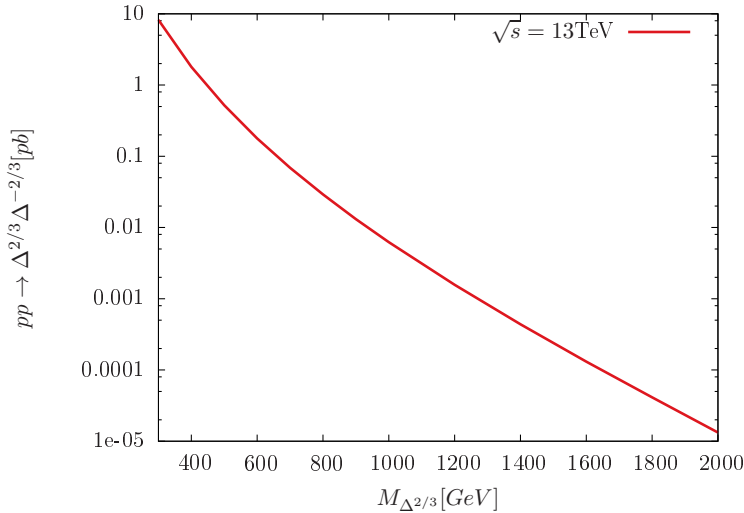


FIG. 1. Pair production cross-section of leptoquarks at the LHC with 13 TeV center-of-mass energy as a function of the leptoquark mass.

coupling. Being mainly QCD driven, the pair production of leptoquarks [63] gets significant corrections from the higher order processes. In Ref. [64], next-to-leading (NLO) order in QCD k -factor for leptoquark pair production at the 13 TeV LHC is estimated to be ~ 1.4 . In our calculation, we have included the k -factor. The QCD pair production cross-section of the leptoquarks ($\sigma(pp \rightarrow \Delta^{+2/3} \Delta^{-2/3})$) as a function of the leptoquark mass ($M_{\Delta^{\pm 2/3}}$) at the LHC with 13 TeV center-of-mass energy is presented in Fig. 1. Being strongly interacting, leptoquark pair production cross-sections are rather large at the LHC as it can be seen from Fig. 1. The pair production cross-section varies from few picobarn to few femtobarn for the LQ mass between few hundred GeV to TeV.

After being produced, leptoquarks decay into a quark-lepton pairs via the Yukawa interactions of Eq. 4. For example, $\Delta^{\pm 2/3}$ can decay into a down type quark and charged lepton pair or a up type quark and right-handed neutrino pair. The decay of $\Delta^{\pm 2/3}$ into a down type quark and charged lepton pair is proportional to Y_L whereas, the decay into a up type quark and right-handed neutrino pair is proportional to Y_R . For simplicity, we have assumed that leptoquark Yukawa matrices are diagonal and leptoquarks can dominantly couple to the third generation of SM fermions³. Similarly, as mentioned earlier, we have also chosen

³ This choice is motivated as leptoquark decaying into a top quark and heavy neutrino results in higher jet, lepton multiplicities and larger missing energy in the final state.

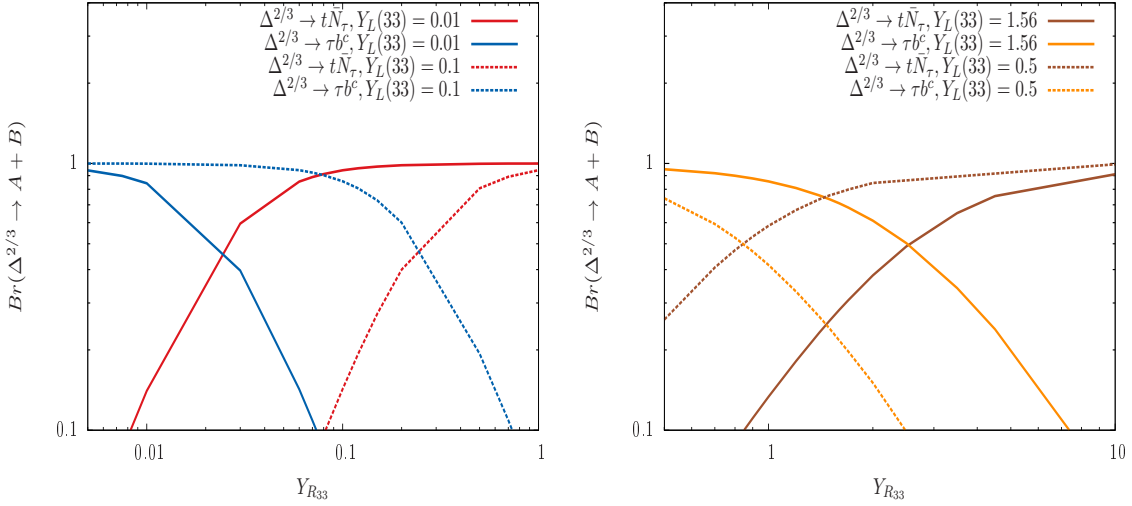


FIG. 2. Branching ratios of $\Delta^{\pm 2/3}$ into tN_τ and $b\tau$ pairs as a function of Y_R^{33} for different values of Y_L^{33} . Left and right panel correspond to 850 GeV and 1 TeV leptoquark masses, as illustrative examples.

the neutrino Yukawa matrix (Y_ν) to be diagonal in order to avoid constraints arising from non-observation of lepton flavor violating decays. As a result of this choice the third generation RH neutrino (which will be denoted as N_τ in the mass basis) can only directly decay into a tau and W-boson or a light ν_τ and Z (with smaller branching ratio) through its left handed components which compels us to look for tau-enriched final states. This will also help us to reduce SM backgrounds, atleast for the signal regions we will be dealing with. We note in passing that keeping the flavor diagonal structure for $Y_{L,R}$, one may obtain μ rich final states for larger values of Y_R^{22} ($Y_R^{22} \gg Y_L^{22}$ and $Y_{L,R}^{22} \gg Y_{L,R}^{33}$), but then one may face relatively difficult task in regard to c -jet tagging.

Thus, in this framework, $\Delta^{+2/3}$ dominantly decays into a top and third generation right-handed neutrino pair (tN_τ) or a bottom quark and tau lepton pair ($b\bar{\tau}$) depending on the relative values of Y_R^{33} and Y_L^{33} , respectively. In Fig. 2, we have presented the branching ratio of $\Delta^{\pm 2/3}$ into tN_τ and $b\tau$ pairs as a function of Y_R^{33} for different values of Y_L^{33} , and write down the analytic expression of the decay widths in the appendix.

Fig. 2 clearly shows that tN_τ decay mode dominates for larger values of Y_R^{33} compared to Y_L^{33} . The off-shell decays for example $\Delta^{2/3} \rightarrow \Delta^{1/3}W^*$ does not occur in this scenario due to mass degeneracy of the two LQs. In order to enhance the production of right handed

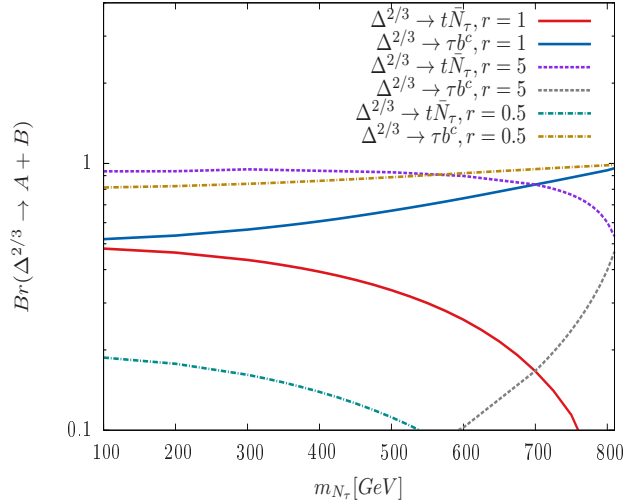


FIG. 3. Variation of branching ratios of $\Delta^{\pm 2/3}$ into tN_τ and $b\tau$ pairs as a function of heavy neutrino mass m_{N_τ} . The LQ mass is set to 1 TeV and $r = \frac{Y_{R33}}{Y_{L33}}$.

neutrinos from the decay of $\Delta^{\pm 2/3}$, smaller Y_L^{33} compared to Y_R^{33} is preferred. Note that, for larger Y_L^{33} , the bounds on $\Delta^{\pm 2/3}$ mass are much stronger from resonance searches in the lepton-jet invariant mass distribution at the LHC [65]. Therefore, in our analysis, we consider $Y_R^{33} > Y_L^{33}$ hence, $\Delta^{\pm 2/3}$ dominantly decays into tN_τ pairs with almost 100% branching ratios.

In addition to the variation w.r.t Yukawa, we also show the variation w.r.t the RH neutrino mass. In Fig. 3, we show the variation of the branching ratios of $\Delta^{2/3}$ with the RH neutrino mass m_{N_τ} . The LQ mass is set to 1 TeV and we define r as the ratio of $\frac{Y_{R33}}{Y_{L33}}$ to delineate the dependence of the branching fraction on the m_{N_τ} . Clearly, $Br(\Delta^{2/3} \rightarrow tN_\tau)$ would be the most dominant channel for $r > 1$. For representation purpose we assume $r = 5$, and we observe that the $Br(\Delta^{2/3} \rightarrow tN_\tau)$ is always 100% if phase space is allowed. The fall in $Br(\Delta^{2/3} \rightarrow tN_\tau)$ occurs near the kinematic threshold $m_{N_\tau} \sim 827$ GeV for the LQ mass 1 TeV. After the kinematic threshold, additional three body modes such as, $\Delta^{2/3} \rightarrow tWl, tZ\nu$ with branching ratio 30–40% also open up. In our subsequent analysis, we work with higher Y_R^{33} , and relatively smaller mass of N_τ as compared to the LQ, so that the two body decay mode $\Delta^{\pm 2/3} \rightarrow tN_\tau$ is almost 100%.

The produced N_τ subsequently decays into a τW pair or a $\nu_\tau Z$ ⁴ pair. Therefore, the pair

⁴ Though the decay widths of N_τ into τW or $\nu_\tau Z$ are suppressed by the small left-handed and right-handed neutrino mixing angle, but in absence of any other decay modes, N_τ decays into τW and $\nu_\tau Z$ pair with 67% and 33% branching ratios, respectively.

production of $\Delta^{\pm 2/3}$ at the LHC gives rise to multiple top-quarks, tau-leptons, W and/or Z -bosons in the final state. Subsequent decays of those heavier SM particles result into multiple leptons, jets and missing transverse energy (E_T) signature at the LHC. Before going into the details of signal and background analysis, let us have a brief discussion on the present status of the heavy neutrino and leptoquark searches in collider and other experiments which lead to our choices of benchmark points for subsequent collider study.

III. PRESENT STATUS, CONSTRAINTS AND CHOICE OF BENCHMARK POINTS

The collider signatures of right-handed neutrinos have been extensively studied in the literature [33, 43, 44, 66–75]. Usually, the search for a heavy Majorana neutrino is driven by lepton number violating final states which provide a smoking-gun signals for such scenarios. However, within the framework of inverse seesaw, the lepton number is broken by the μ -parameter which is extremely small and therefore, the usual same-sign dilepton signal is expected to be much weaker in this scenario compared to a trilepton signal [39]. In fact, the smallness of μ results in suppression of any lepton number violating (LNV) processes in this framework. Thus in the considered scenario, the first-generation Dirac neutrino Yukawa coupling Y_ν^{11} , which is highly constrained for Type-I seesaw mechanism from non-observation of neutrino-less double beta decay ($0\nu\beta\beta$) [38], remains practically unconstrained. The experimental collaborations have put constraints on the heavy Majorana neutrino masses depending on its choice of Dirac neutrino Yukawa couplings from the search of same flavor opposite-sign dilepton final state [76–81]. In the inverse seesaw scenario, these constraints are trivially satisfied. Comparatively, some other final states with various lepton-jet multiplicities can provide a more stringent constraint on the inverse seesaw scenario that can probe a mixing angle up to $\sim 10^{-2}$ for a heavy neutrino mass around 200 GeV at 14 TeV run of the LHC with a luminosity around 1000 fb^{-1} [39]. In this work, we aim to probe up to a much higher RH neutrino mass range. This is achievable, as our RH neutrino production is not limited by the active-sterile mixing which is further constrained from precision studies [17, 82–85]. Instead, the heavy neutrino is produced from leptoquark decays, that has strong interaction. This helps to obtain a relatively larger RH neutrino production cross-section. Another potential source of the constraints on the neutrino sector may arise from the lepton

flavor violating (LFV) decays that arise due to non-diagonal Y_ν or M_R . In this analysis, we consider these two matrices strictly diagonal which leads to vanishing contribution of the new physics contribution to the LFV decays.

Experimental collaborations have also searched for any possible hints for scalar leptoquarks at the LHC [86, 87]. The favored final state to look for these exotic particles has been $\ell\ell jj$, where, $\ell = e, \mu, \tau$. The non-observation of any new physics events have ruled out LQ up to masses as large as 1100 GeV. However, these existing limits are subjected to a particular choice of Y_L that forces the leptoquarks to decay dominantly into a charged lepton and a light (or bottom) quark. In this work, however, we intend to explore a different coupling of the LQ, namely, Y_R which forces the LQ to decay via the heavy neutrinos. Therefore, taking a clue from the obtained branching ratio distribution of the LQs as shown in Fig. 2, we keep Y_L smaller in comparison to Y_R for all our benchmark points so that relatively lighter LQ masses can be probed which are still allowed by the LHC. However, the leptoquark decaying via heavy neutrinos can give rise to the same kind of multi lepton signals which has usually been studied in the context of supersymmetric searches [88–90]. So far all such search results have turned out to be consistent with the SM predictions and hence these results can constrain the LQ as well as heavy neutrino masses in our scenario.

As has been mentioned, in this work, we have considered the pair production of $\Delta^{\pm 2/3}$ and its subsequent decay into a top and a heavy neutrino. Hence, the collider phenomenological aspects of our study are determined by five parameters namely, leptoquark mass ($m_{\Delta^{\pm 2/3}}$), its couplings $Y_{L,R}^{33}$, right-handed neutrino mass (m_{N_τ}) and its coupling m_D^{33} . The pair-production cross-section $\sigma(\Delta^{\pm 2/3}\Delta^{\mp 2/3})$ is determined by the choice of $m_{\Delta^{\pm 2/3}}$ and its couplings. While, relative strength of Y_R^{33} and Y_L^{33} determines the decay of $\Delta^{\pm 2/3}$ into right-handed neutrino (N_τ), the mass splitting between $\Delta^{\pm 2/3}$ - N_τ determines the shape of characteristic signal distributions. In order to present the numerical results of our analysis, we have chosen three benchmark points (BP). The relevant parameters for the collider phenomenology for those three BPs are listed in Tables 2 and 3. We also present a bench-mark point (BP2 in Table 3) which can potentially explain B - physics anomalies as mentioned earlier. In order to get a large $BR(\Delta^{\pm 2/3} \rightarrow tN_\tau)$, only large values of Y_R^{33} are allowed which nearly saturates the perturbative limits $\sim 4\pi$ even at the TeV scale. However, we recall that LQs are always associated with larger symmetry. Assuming a larger gauge group at the TeV scale can potentially help to avoid Landau-pole problem due to large value of Y_R^{33} .

Parameters	BP1	BP2	BP3
m_D^{ii}	(0.1, 0.1, 0.1)	(10^{-9} , 10^{-9} , 0.1)	(0.1, 0.1, 0.1)
M_R^{ii} (GeV)	(1000.0, 1000.0, 400.0)	(10^{-6} , 10^{-6} , 600)	(1000.0, 1000.0, 800.0)
μ_X (eV)	$\begin{pmatrix} 9.233 & 15.141 & 2.799 \\ 15.141 & 52.874 & 22.228 \\ 2.799 & 22.228 & 15.921 \end{pmatrix}$	$\begin{pmatrix} 0.144 & 0.237 & 0.525 \\ 0.237 & 0.826 & 4.168 \\ 0.525 & 4.168 & 35.821 \end{pmatrix}$	$\begin{pmatrix} 14.427 & 23.658 & 6.998 \\ 23.658 & 82.616 & 55.569 \\ 6.998 & 55.569 & 63.683 \end{pmatrix}$
Resulting PMNS	$\begin{pmatrix} 0.810 & 0.507 & 0.295 \\ 0.567 & 0.550 & 0.612 \\ 0.148 & 0.663 & 0.733 \end{pmatrix}$	$\begin{pmatrix} 0.806 & 0.493 & 0.284 \\ 0.548 & 0.556 & 0.610 \\ 0.143 & 0.647 & 0.740 \end{pmatrix}$	$\begin{pmatrix} 0.806 & 0.511 & 0.297 \\ 0.573 & 0.549 & 0.608 \\ 0.148 & 0.661 & 0.736 \end{pmatrix}$

TABLE 2. m_D and M_R taken as inputs, μ_X is the resulting matrix derived such that the oscillation parameters are in agreement.

Table 2 shows the choices of the neutrino sector parameters, m_D and M_R and the resulting μ_X after fitting the neutrino oscillation data as mentioned in Section II A. We have also presented the obtained light 3×3 neutrino mass matrices which are in good agreement with the allowed PMNS matrix elements. Non-diagonal structure of μ_X reflects to the fact that we have assumed diagonal Y_ν^{ii} , hence m_D^{ii} to suppress lepton flavor violating observables. In the present context, the effective production cross-section of the right handed neutrinos have been considerably larger, thanks to larger productions for LQs ($\Delta^{(2/3)}$) and their decays to tN_τ with almost 100% branching ratio. Table 3 shows our choices of LQ ($\Delta^{(2/3)}$) masses

Benchmarks	$m_{\Delta^{(2/3)}} (GeV)$	$m_{N_\tau} (GeV)$	Y_L^{ii}	Y_R^{ii}	$\sigma_{\Delta^{(2/3)}\bar{\Delta}^{(2/3)}} (fb)$
BP1	850.0	400.0	(0.0, 10^{-3} , 10^{-3})	(0.0, 10^{-3} , 0.1)	18.760
BP2	1000.0	600.0	(0.0, 10^{-3} , 1.5)	(0.0, 10^{-3} , 12.56)	6.342
BP3	1200.0	800.0	(0.0, 10^{-3} , 10^{-3})	(0.0, 10^{-3} , 0.1)	1.512

TABLE 3. Relevant parameters and production cross-section (including the k-factor) of leptoquarks at LHC, for 13 TeV c.m.energy.

and their relevant couplings along with their pair production cross-section for the three benchmark points. We now proceed to discuss our collider analysis of the leptoquarks decaying via heavy neutrinos yielding various possible novel signal regions.

IV. COLLIDER ANALYSIS AND RESULTS

As has already been discussed, our primary focus is on the interaction induced by the Yukawa couplings of right-handed neutrinos with the leptoquarks which give rise to interesting signals at the LHC. Leptoquarks, being strongly interacting, are copiously produced at hadron colliders. Therefore, in the framework of leptoquark model, the production of right handed neutrinos could be enhanced significantly. Moreover, the decay of leptoquarks are usually accompanied by hard jets and/or leptons which could enhance the efficiency of signal selection criteria to reduce the SM background. With the LHC running at its near kinematic threshold, at $\sqrt{s} = 13$ TeV, one also has to deal with the large hadronic backgrounds while looking for any new physics signal. One way to avoid this menace is to look for more and more lepton enriched final states which naturally tend to reduce these unwanted background contributions. We have, therefore, focussed to identify the signal regions in a way so that the maximum number of hard leptons, like-sign or otherwise, are identified in the final state while not tagging all the b -jets and τ -jets arising from the cascades in order to maximize the signal rates. In the framework of the present model, different signal regions (SR) can be defined with multiple leptons when $\Delta^{\pm 2/3} \rightarrow tN_\tau$ and $N_\tau \rightarrow \tau W$ or $\nu_\tau Z$ are followed by the leptonic decay of both the top quarks and the gauge bosons present in the cascade.

$$\begin{aligned}
 pp &\rightarrow \Delta^{\pm 2/3} \Delta^{\mp 2/3} \rightarrow (t\bar{N}_\tau)(\bar{t}N_\tau) \\
 &\rightarrow b\bar{b}W^+W^-\tau^+\tau^-W^+W^- \\
 &\rightarrow b\bar{b}W^+W^-\nu_\tau\bar{\nu}_\tau ZZ \\
 &\rightarrow b\bar{b}W^+W^-\tau^+\nu_\tau W^-Z
 \end{aligned}
 \tag{10}$$

The above three possible decay chains can potentially give rise to maximum six leptons in the final state. Any final state with such a large lepton multiplicity will be a very clean signal devoid of SM background. However, that will require both the N_τ s to decay via the Z-boson which has a suppressed branching ratio compared to its W-decay mode. Moreover, the Z-boson decay branching ratios to the electrons and muons are also suppressed. Hence we restrict ourselves to signal regions with at least three or four leptons in the final state. Note that, here we focus on the RH neutrino decay to τ lepton. The e, μ states are mostly generated from the gauge boson decays. Another interesting signal region (SR) can be constructed from the first and third cascade decays shown in Eq. 10 when two of the same-sign W-bosons decay leptonically and the other W and (or) Z-bosons decay hadronically.

This will result into a same-sign dilepton (SSD) signal along with multiple jets and \cancel{E}_T . Such a SSD signal is expected to be different from the usual heavy neutrino signals both in terms of jet multiplicity and \cancel{E}_T distribution.

For a detailed collider simulation, we have generated parton level events using MadGraph5 and subsequently passed the events into Pythia (v6.4.28) [91] for simulating initial state radiation/final state radiation (ISR/FSR), decay of the heavy particles and hadronisation of the final state quarks. In order to reconstruct the physics objects like, jets, leptons, photons and missing transverse energy, we have used the fast detector simulator Delphes-v3.3.3 [92–94]. The jets are reconstructed by anti- k_t algorithm [95] implemented in Fastjet package [95–97] with a cone of $\Delta R = 0.4$ and minimum transverse momentum of 20 GeV. The tagging and mistagging efficiencies of b -jet and τ -jet have been incorporated according to the latest ATLAS studies in this regard [98] in Delphes3. After the object reconstruction, leptons with $p_T^l > 10$ GeV and $|\eta^l| < 2.5$ and jets with $p_T^j > 20$ GeV and $|\eta^j| < 2.5$ are considered for the further event selection. Furthermore, the electrons and muons satisfying the p_T^l criteria have been selected with 95% and 85% efficiencies for $|\eta^l| < 1.5$ and $1.5 < |\eta^l| < 2.5$ respectively. Finally, the b and τ jets are tagged with $p_T > 20$ GeV while the rest of the jets are tagged with different p_T requirements of our signal regions following the ATLAS event selection criteria as in Refs. [89, 90].

Multiple sources of missing energy throughout the cascade and the large multiplicity of both jets and(or) leptons are likely to produce hard \cancel{E}_T and M_{EFF} distributions, where $M_{EFF} = \sum_i p_{T_i}^j + \sum_i p_{T_i}^l + \cancel{E}_T$. In Fig. 4, we have shown these kinematic distributions for the three benchmark points introduced in Section III.

The distributions in Fig. 4 are obtained for final states containing at least two leptons. The blue, red and black lines represent BP1, BP2 and BP3 respectively. As expected, the hardness of the distributions increases with increasing leptoquark and heavy neutrino masses. The final state should also consist a large number of jets including multiple b and τ -jets. Tagging the b/τ -jets can reduce the SM backgrounds significantly. The large QCD background at the LHC makes it difficult for any new physics signal with multiple jets to be observed. Tagging additional b/τ -jets helps to reduce this background very effectively. Top-quark associated production channels also give rise to large background contributions which can be minimised by demanding a τ -jet in the final states. However, the detection efficiencies of b/τ -jets vary with their p_T s and hence tagging all the b and (or) τ -jets can also

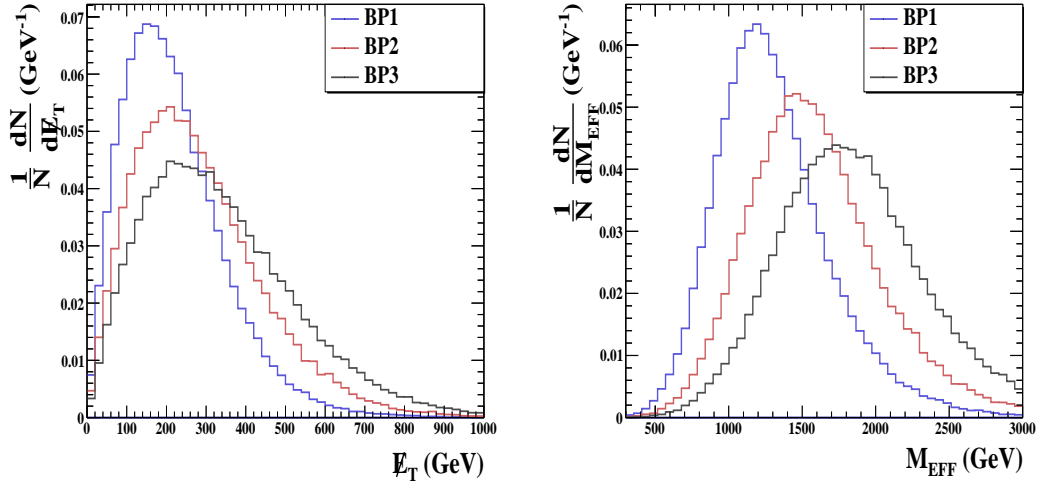


FIG. 4. Normalised distributions of \cancel{E}_T and M_{EFF} for final states consisting of at least two leptons corresponding to the three benchmark points.

reduce the signal rates considerably. Taking into account all these factors, we define four SRs as shown in Table 4. We have categorised the choice of lepton and jet multiplicities

Signal	C0						C1	C2
	N_ℓ	N_j	N_b	N_τ	p_T^j (GeV)	$p_T^{b/\tau}$ (GeV)	\cancel{E}_T (GeV)	M_{EFF} (GeV)
SR3Lb	≥ 3	≥ 4	≥ 1	-	> 40	> 20	> 200	> 600
SR3Lbt	≥ 3	≥ 4	≥ 1	≥ 1	> 40	> 20	> 200	> 600
SR4Lbt	≥ 4	-	≥ 1	≥ 1	> 40	> 20	> 200	> 600
SRSS2Lb	≥ 2	≥ 4	≥ 1	-	> 50	> 20	> 150	≥ 550

TABLE 4. The four different signal regions with lepton, jet multiplicities and kinematic cuts.

and their p_T requirement of the jets, \cancel{E}_T and M_{EFF} under **C0**, **C1** and **C2** respectively as shown in the table.

For most of the signal regions focus on the large lepton and jet multiplicity and the hard \cancel{E}_T and M_{EFF} distributions to achieve a good signal to background ratio. Among the first three SRs, **SR3Lb** and **SR3Lbt** are expected to have some SM background contributions while **SR4Lbt** is likely to be a much cleaner channel. As mentioned before, any lepton number violating signals are suppressed in the framework of the inverse seesaw scenario due

to the smallness of μ_X . Hence the usual SSD signal is not viable to probe for inverse seesaw extended SM. However, here one can obtain a different kind of same-sign dilepton signal as shown in **SRSS2Lb**, where the same-sign criteria is imposed on the events with exactly two leptons in the final state. Such a signal region can, therefore, be a distinguishing feature for such a scenario. The choice of our signal regions are motivated from some experimental studies with final states consisting of multiple jets and leptons in the context of Supersymmetry [88–90]. There are multiple signal regions studied in these works, which can be relevant to our scenario. Therefore, we have checked the consistency of our chosen benchmark points with these experimental results using CheckMATE [99, 100] which determines whether a chosen model parameter space is excluded or not at 95% confidence level [101] by comparing it to the relevant experimental analyses.⁵

The obtained signal cross-sections at 13 TeV center-of-mass energy are presented in Table 5 with cut-flow numbers for the signal regions and cuts **C0** - **C2** as defined in Table 4 corresponding to the three BPs defined in Table 3. Irrespective of the choice of different signal regions, the M_{EFF} cut (**C2**) does not affect the signal cross-sections for any of the benchmark points. This is quite expected as Fig. 4 clearly shows our choice of the \cancel{E}_T cut (**C1**) automatically pushes the phase space to a hard kinematic region where the M_{EFF} cut is trivially satisfied. However, **C2** is very useful to reduce the SM backgrounds for these signal regions as mentioned in [89, 90].

Signal Region	Signal cross-section (fb)								
	BP1			BP2			BP3		
	C0	C1	C2	C0	C1	C2	C0	C1	C2
SR3Lb	0.376	0.181	0.181	0.130	0.081	0.081	0.330	0.024	0.024
SR3Lbt	0.137	0.062	0.062	0.047	0.027	0.027	0.012	0.009	0.009
SR4Lbt	0.016	0.007	0.007	0.006	0.003	0.003	0.002	0.001	0.001
SRSS2Lb	0.924	0.598	0.598	0.320	0.245	0.245	0.080	0.066	0.066

TABLE 5. Cut-flow table for signal cross-sections with the cuts mentioned in Table 4 for the different SRs and BPs at the LHC at 13 TeV center-of-mass energy.

⁵ The analyses of Ref.[89] have not yet been included in CheckMATE. We have checked consistency of our benchmark points with these results using our own code.

- The signal region **SR3Lb** with three or more leptons and at least one tagged b -jet has also been studied by the ATLAS Collaboration although in a different context [89]. They estimated a combined SM background cross-section of 0.56 fb. In absence of any significant deviation from the SM background prediction, the ATLAS collaboration has derived an upper bound of 0.41 fb on new physics tri-lepton cross-section in **SR3Lb** signal region. As the numbers in Table 5 suggest, all our benchmark points are well within this experimental bound. We have also checked that the ATLAS study of **SR3Lb** imposes a lower bound of about 700 GeV on the mass of the 3rd generation leptoquark if it dominantly decays into a top-quark and a heavy neutrino in the framework of the present model. Taking into account the SM background contribution, one can obtain a statistical significance⁶ of 3σ for BP1 at an integrated luminosity (L) of $\sim 200 \text{ fb}^{-1}$. For BP2, with higher LQ mass, in order to achieve similar statistical significance, one needs $L \sim 900 \text{ fb}^{-1}$. BP3 is unlikely to be probed in this SR even at a relatively high luminosity of $L \sim 3000 \text{ fb}^{-1}$.
- Demanding at least one additional τ -jet (*i.e.*, the SR **SR3Lbt**) reduces the signal cross-section to 0.062 fb for BP1. However, demanding an extra τ -tagged jet on the top of **SR3Lb** reduces the SM background cross-section at least by a factor of α_W . Thus, even the ~ 12 events expected at $L \sim 200 \text{ fb}^{-1}$ for BP1 is relatively background free and can act as a complementary channel to **SR3Lb**. This SR can be more economical for BP2 and BP3 compared to the previous one. As the numbers in Table 5 suggest, both these benchmark points can be probed below and around $L = 1000 \text{ fb}^{-1}$ respectively.
- **SR4Lbt** is even a more cleaner channel to probe for the present scenario. However, as the numbers suggest, in order to get some signal events ($N_{sig} \sim 7$ for BP1) in this signal region, one has to go for high luminosity $L \sim 1000 \text{ fb}^{-1}$. Thus this signal region can only serve as a complementary channel to the previous two if any excess of events are found in either of them. For LQ masses around 1000 GeV and above, as in BP2 and BP3, this SR does not look promising enough due to extremely small signal cross-section.

⁶ Statistical significance, $\mathcal{S} = \frac{s}{\sqrt{s+b}}$, where s =number of signal events and b =number of background events.

- The signal region **SRSS2Lb** has been studied in the context of supersymmetry at the LHC. Here we have used the same set of selection criteria and kinematic cuts as the ATLAS collaboration [90] to obtain the signal cross-section. The experimental upper limit on new physics cross-section in this signal region remains at 2.8 fb which is much larger than that obtained for any of the benchmark points of our choice. Although the SM background contribution in this channel is expected to be the largest compared to the other **SRs**, the large signal cross-section makes it the most promising channel to probe at the LHC. The ATLAS collaboration quoted the total SM background contribution as 1.406 fb [90]. This leads to a statistical significance of 3σ at $L \sim 55 \text{ fb}^{-1}$ for BP1 which means this parameter space can immediately be probed with the accumulated data at the LHC at present. To achieve similar statistical significance for BP2 and BP3 one requires $L \sim 250 \text{ fb}^{-1}$ and 3000 fb^{-1} respectively.

From the above, it is evident that a lighter LQ mass and lighter RH neutrino, such as $M_{\Delta_{2/3}} = 850, m_{N_\tau} = 400 \text{ GeV}$ can be probed in very near future with the data already accumulated at the LHC through at least two same-sign leptons, multi-jet and one tagged b -jet in the final state. Even a heavier neutrino ($\sim 600 \text{ GeV}$) can be probed in association with a $\sim 1000 \text{ GeV}$ leptoquark mass at a relatively lower luminosity of 250 fb^{-1} in this final state. To probe higher mass ranges, as represented by BP3, the HL-LHC run is required. Among the other **SRs**, **SR3Lb** and **SR3Lbt** turn out to be the other viable options. However, they will be relevant only if some hint of new physics is obtained at lower luminosity via **SRSS2Lb**. Besides, it also provides us with a nice distinguishing feature that can be used to differentiate an usual inverse seesaw extended SM scenario from the present one. Note that, almost two third contribution of the signal cross-section in this **SR** arises from same-sign two-lepton final state, a contribution which is expected to be negligible in the usual inverse seesaw extended SM.

V. CONCLUSION & OUTLOOK

In this work, we have considered a minimal extension of the SM that can (i) produce neutrino masses and mixing angles and (ii) explain B -physics anomalies. We consider a scalar LQ with the hypercharge $Y = \frac{1}{6}$ and embed it in a inverse-seesaw framework with TeV scale or even lighter sterile neutrinos. Presence of a dominant flavor diagonal LQ- ν_R coupling

can greatly enhance the effective production cross-section of the heavy neutrino states in comparison to the canonical sterile neutrino production through charged/neutral current weak interactions. We have studied a rather unexplored decay mode of the leptoquark, i.e, to a top quark and heavy right handed neutrino with almost 100% Br. This results in various multi lepton signals associated with multiple jets (including b and τ -jets) and missing transverse energy. We have explored four such signal regions and carried out a comparative analysis aimed at probing heavy neutrino masses. We find that while a RH neutrino of mass 400 GeV can immediately be probed at the LHC with at least one same-sign dilepton and multi-jet signal, a relatively heavier neutrino mass scales such as 800 GeV can be probed in the high luminosity run of LHC. We have also observed that a mass bound of 700 GeV on the LQ mass can be derived following the ATLAS 13 TeV search in trilepton channel associated with multiple jets and at least one b-tagged jet provided the LQ decays dominantly into a top-quark and a heavy neutrino.

We have also presented a same-sign dilepton signal region which is expected to yield a much smaller event rate at the collider in the inverse seesaw extended SM. However, in the presence of leptoquarks where the heavy neutrinos are produced from the decay of these colored particles alongside top quarks, we have shown that one can expect significant event rates in this same-sign dilepton channel associated with multiple jets and missing energy.

Qualitatively all these can be considered as nice distinguishing features between the conventional inverse seesaw and the leptoquark associated inverse seesaw model. Quantatively, one can observe that much larger mass scale for heavy neutrinos can be reached through the aforesaid signal regions, specially via same-sign dileptons. Finally, allowing small off-diagonal structure in the $LQ-\nu_R$ coupling may lead to new avenues to LHC physics and flavor violations which requires a dedicated study.

ACKNOWLEDGMENTS

KG and MM acknowledges the support of DST-INSPIRE FACULTY research grant. The work of SM is partially supported by funding available from the Department of Atomic Energy, Government of India, for the Regional Centre for Accelerator-based Particle Physics (RECAPP), Harish-Chandra Research Institute. SM acknowledges the hospitality of Institute of Physics, Bhubaneswar during initial phase of the work.

APPENDIX

Relevant decays of the Leptoquark:

Below, we write down the different two body decays of the LQ, relevant for our work.

$$\Gamma(\Delta^{2/3} \rightarrow t\bar{N}_\tau) = \frac{(Y_R^{33})^2((V_N^{53})^2 + (V_N^{63})^2)}{16\pi(m_{\Delta(2/3)})^3}((m_{\Delta(2/3)})^2 - m_{N_\tau}^2 - m_t^2) \times \sqrt{((m_{\Delta(2/3)})^2 - (m_{N_\tau} + m_t)^2)((m_{\Delta(2/3)})^2 - (m_{N_\tau} - m_t)^2)} \quad (11)$$

$$\Gamma(\Delta^{2/3} \rightarrow b\bar{\tau}) = \frac{(Y_L^{33})^2}{16\pi(m_{\Delta(2/3)})^3}((m_{\Delta(2/3)})^2 - m_b^2 - m_\tau^2) \times \sqrt{((m_{\Delta(2/3)})^2 - (m_b + m_\tau)^2)((m_{\Delta(2/3)})^2 - (m_b - m_\tau)^2)} \quad (12)$$

where, V_N^{ij} ($i, j = 1, \dots, 6$) diagonalises the heavy neutrino mass matrix (\mathcal{M}_N) written in the basis $\{\nu_R^1, \nu_R^2, \nu_R^3, X^1, X^2, X^3\}$. Note that all the six heavy neutrino masses are driven by the choices of M_R^{ii} since all the diagonal entries of \mathcal{M}_N are essentially zero ($\mu_X \ll M_R$). Upon diagonalisation of \mathcal{M}_N , we obtain three pairs of mass degenerate heavy neutrino states with masses $\simeq M_R^{11}$, M_R^{22} and M_R^{33} respectively. While writing V_N , the eigenvalues are arranged from heavy to light order. The fifth and sixth eigenvalues (mass degenerate) are driven by the choice of M_R^{33} since by our choice, $M_R^{33} < M_R^{11}, M_R^{22}$. Only V_N^{53} and V_N^{63} elements are of importance for the decay $\Delta^{2/3} \rightarrow t\bar{N}_\tau$ since the relevant term in the Lagrangian is $Y_R^{ij} \bar{u}_L^i \nu_R^j \Delta^{(2/3)}$ and we have chosen to work with diagonal Y_R . m_t , m_b and m_τ are the masses of top quark, bottom quark and τ -lepton respectively.

-
- [1] <https://twiki.cern.ch/twiki/bin/view/AtlasPublic>, .
 - [2] <https://twiki.cern.ch/twiki/bin/view/CMSPublic>, .
 - [3] M. C. Gonzalez-Garcia and M. Maltoni, *Phys. Rept.* **460**, 1 (2008), [arXiv:0704.1800](https://arxiv.org/abs/0704.1800) [hep-ph].
 - [4] M. C. Gonzalez-Garcia, M. Maltoni, and T. Schwetz, *Nucl. Phys.* **B908**, 199 (2016), [arXiv:1512.06856](https://arxiv.org/abs/1512.06856) [hep-ph].
 - [5] P. Minkowski, *Phys. Lett.* **B67**, 421 (1977).
 - [6] R. N. Mohapatra and G. Senjanovic, *Phys. Rev. Lett.* **44**, 912 (1980).
 - [7] M. Gell-Mann, P. Ramond, and R. Slansky, Print-80-0576 (CERN).

- [8] T. Yanagida, In Proceedings of the Workshop on the Baryon Number of the Universe and Unified Theories, Tsukuba, Japan, 13-14 Feb 1979.
- [9] S. L. Glashow, NATO Adv. Study Inst. Ser. B Phys. **59**, 687 (1980).
- [10] J. Schechter and J. W. F. Valle, *Phys. Rev.* **D25**, 774 (1982).
- [11] J. Schechter and J. W. F. Valle, *Phys. Rev.* **D22**, 2227 (1980).
- [12] S. Weinberg, *Phys. Rev. Lett.* **43**, 1566 (1979).
- [13] S. Weinberg, *Phys. Rev.* **D22**, 1694 (1980).
- [14] M. Magg and C. Wetterich, *Phys. Lett.* **94B**, 61 (1980).
- [15] T. P. Cheng and L.-F. Li, *Phys. Rev.* **D22**, 2860 (1980).
- [16] R. Foot, H. Lew, X. G. He, and G. C. Joshi, *Z. Phys.* **C44**, 441 (1989).
- [17] S. Antusch and O. Fischer, *JHEP* **05**, 053 (2015), [arXiv:1502.05915 \[hep-ph\]](#).
- [18] R. N. Mohapatra, *Phys. Rev. Lett.* **56**, 561 (1986).
- [19] S. Nandi and U. Sarkar, *Phys. Rev. Lett.* **56**, 564 (1986).
- [20] R. N. Mohapatra and J. W. F. Valle, *Proceedings, 23RD International Conference on High Energy Physics, JULY 16-23, 1986, Berkeley, CA*, *Phys. Rev.* **D34**, 1642 (1986).
- [21] G. 't Hooft, *Recent Developments in Gauge Theories. Proceedings, Nato Advanced Study Institute, Cargese, France, August 26 - September 8, 1979*, *NATO Sci. Ser. B* **59**, 135 (1980).
- [22] J. Cao, X. Guo, Y. He, L. Shang, and Y. Yue, (2017), [arXiv:1707.09626 \[hep-ph\]](#).
- [23] B. Karmakar and A. Sil, *Phys. Rev.* **D96**, 015007 (2017), [arXiv:1610.01909 \[hep-ph\]](#).
- [24] R. Sinha, R. Samanta, and A. Ghosal, *Phys. Lett.* **B759**, 206 (2016), [arXiv:1508.05227 \[hep-ph\]](#).
- [25] E. Arganda, M. J. Herrero, X. Marcano, and C. Weiland, *Phys. Rev.* **D93**, 055010 (2016), [arXiv:1508.04623 \[hep-ph\]](#).
- [26] A. Abada, D. Das, A. Vicente, and C. Weiland, *JHEP* **09**, 015 (2012), [arXiv:1206.6497 \[hep-ph\]](#).
- [27] A. Abada, D. Das, and C. Weiland, *JHEP* **03**, 100 (2012), [arXiv:1111.5836 \[hep-ph\]](#).
- [28] A. Abada, G. Bhattacharyya, D. Das, and C. Weiland, *Phys. Lett.* **B700**, 351 (2011), [arXiv:1011.5037 \[hep-ph\]](#).
- [29] E. Arganda, M. J. Herrero, X. Marcano, and C. Weiland, *Phys. Rev.* **D91**, 015001 (2015), [arXiv:1405.4300 \[hep-ph\]](#).

- [30] E. Arganda, M. J. Herrero, X. Marcano, and C. Weiland, *Phys. Lett.* **B752**, 46 (2016), [arXiv:1508.05074 \[hep-ph\]](#).
- [31] V. De Romeri, M. J. Herrero, X. Marcano, and F. Scarcella, *Phys. Rev.* **D95**, 075028 (2017), [arXiv:1607.05257 \[hep-ph\]](#).
- [32] E. Arganda, M. Herrero, X. Marcano, R. Morales, and A. Szyrkman, *Phys. Rev.* **D95**, 095029 (2017), [arXiv:1612.09290 \[hep-ph\]](#).
- [33] C.-Y. Chen and P. S. B. Dev, *Phys. Rev.* **D85**, 093018 (2012), [arXiv:1112.6419 \[hep-ph\]](#).
- [34] A. Das and N. Okada, *Phys. Rev.* **D88**, 113001 (2013), [arXiv:1207.3734 \[hep-ph\]](#).
- [35] P. Bandyopadhyay, E. J. Chun, H. Okada, and J.-C. Park, *JHEP* **01**, 079 (2013), [arXiv:1209.4803 \[hep-ph\]](#).
- [36] P. S. B. Dev, A. Pilaftsis, and U.-k. Yang, *Phys. Rev. Lett.* **112**, 081801 (2014), [arXiv:1308.2209 \[hep-ph\]](#).
- [37] A. Das, P. S. Bhupal Dev, and N. Okada, *Phys. Lett.* **B735**, 364 (2014), [arXiv:1405.0177 \[hep-ph\]](#).
- [38] F. F. Deppisch, P. S. Bhupal Dev, and A. Pilaftsis, *New J. Phys.* **17**, 075019 (2015), [arXiv:1502.06541 \[hep-ph\]](#).
- [39] A. Das and N. Okada, *Phys. Rev.* **D93**, 033003 (2016), [arXiv:1510.04790 \[hep-ph\]](#).
- [40] S. Mondal and S. K. Rai, *Phys. Rev.* **D94**, 033008 (2016), [arXiv:1605.04508 \[hep-ph\]](#).
- [41] S. Banerjee, P. S. B. Dev, A. Ibarra, T. Mandal, and M. Mitra, *Phys. Rev.* **D92**, 075002 (2015), [arXiv:1503.05491 \[hep-ph\]](#).
- [42] A. Das, (2017), [arXiv:1701.04946 \[hep-ph\]](#).
- [43] D. Alva, T. Han, and R. Ruiz, *JHEP* **02**, 072 (2015), [arXiv:1411.7305 \[hep-ph\]](#).
- [44] C. Degrande, O. Mattelaer, R. Ruiz, and J. Turner, *Phys. Rev.* **D94**, 053002 (2016), [arXiv:1602.06957 \[hep-ph\]](#).
- [45] I. DorÅąner, S. Fajfer, A. Greljo, J. F. Kamenik, and N. KoÅąnik, *Phys. Rept.* **641**, 1 (2016), [arXiv:1603.04993 \[hep-ph\]](#).
- [46] J. C. Pati and A. Salam, *Phys. Rev.* **D10**, 275 (1974), [Erratum: *Phys. Rev.*D11,703(1975)].
- [47] H. Georgi and S. L. Glashow, *Phys. Rev. Lett.* **32**, 438 (1974).
- [48] H. Georgi, *PARTICLES AND FIELDS 1974: Proceedings of the Williamsburg Meeting of APS/DPF*, *AIP Conf. Proc.* **23**, 575 (1975).
- [49] H. Fritzsch and P. Minkowski, *Annals Phys.* **93**, 193 (1975).

- [50] W. Altmannshofer, M. Carena, and A. Crivellin, *Phys. Rev.* **D94**, 095026 (2016), [arXiv:1604.08221 \[hep-ph\]](#).
- [51] D. BeÄDireviÄĜ, S. Fajfer, N. KoÅanik, and O. Sumensari, *Phys. Rev.* **D94**, 115021 (2016), [arXiv:1608.08501 \[hep-ph\]](#).
- [52] D. BeÄDireviÄĜ, S. Fajfer, and N. KoÅanik, *Phys. Rev.* **D92**, 014016 (2015), [arXiv:1503.09024 \[hep-ph\]](#).
- [53] I. DorÅaner, S. Fajfer, N. KoÅanik, and I. NiÅandÅjiÄĜ, *JHEP* **11**, 084 (2013), [arXiv:1306.6493 \[hep-ph\]](#).
- [54] A. Abada and M. Lucente, *Nucl. Phys.* **B885**, 651 (2014), [arXiv:1401.1507 \[hep-ph\]](#).
- [55] P. C. with Olcyr Sumensari, .
- [56] N. D. Christensen and C. Duhr, *Comput. Phys. Commun.* **180**, 1614 (2009), [arXiv:0806.4194 \[hep-ph\]](#).
- [57] A. Alloul, N. D. Christensen, C. Degrande, C. Duhr, and B. Fuks, *Comput. Phys. Commun.* **185**, 2250 (2014), [arXiv:1310.1921 \[hep-ph\]](#).
- [58] J. Alwall, M. Herquet, F. Maltoni, O. Mattelaer, and T. Stelzer, *JHEP* **06**, 128 (2011), [arXiv:1106.0522 \[hep-ph\]](#).
- [59] J. Alwall, R. Frederix, S. Frixione, V. Hirschi, F. Maltoni, O. Mattelaer, H. S. Shao, T. Stelzer, P. Torrielli, and M. Zaro, *JHEP* **07**, 079 (2014), [arXiv:1405.0301 \[hep-ph\]](#).
- [60] R. D. Ball *et al.*, *Nucl. Phys.* **B867**, 244 (2013), [arXiv:1207.1303 \[hep-ph\]](#).
- [61] R. D. Ball *et al.* (NNPDF), *JHEP* **04**, 040 (2015), [arXiv:1410.8849 \[hep-ph\]](#).
- [62] <https://cp3.irmp.ucl.ac.be/projects/madgraph/wiki/FAQ-General-13>, .
- [63] B. Diaz, M. Schmaltz, and Y.-M. Zhong, *JHEP* **10**, 097 (2017), [arXiv:1706.05033 \[hep-ph\]](#).
- [64] T. Mandal, S. Mitra, and S. Seth, *Phys. Rev.* **D93**, 035018 (2016), [arXiv:1506.07369 \[hep-ph\]](#).
- [65] C. Collaboration (CMS), (2016).
- [66] W.-Y. Keung and G. Senjanovic, *Phys. Rev. Lett.* **50**, 1427 (1983).
- [67] A. Datta, M. Guchait, and A. Pilaftsis, *Phys. Rev.* **D50**, 3195 (1994), [arXiv:hep-ph/9311257 \[hep-ph\]](#).
- [68] F. M. L. Almeida, Jr., Y. do Amaral Coutinho, J. A. Martins Simoes, and M. A. B. do Vale, *Phys. Rev.* **D62**, 075004 (2000), [arXiv:hep-ph/0002024 \[hep-ph\]](#).
- [69] O. Panella, M. Cannoni, C. Carimalo, and Y. N. Srivastava, *Phys. Rev.* **D65**, 035005 (2002), [arXiv:hep-ph/0107308 \[hep-ph\]](#).

- [70] T. Han and B. Zhang, *Phys. Rev. Lett.* **97**, 171804 (2006), [arXiv:hep-ph/0604064 \[hep-ph\]](#).
- [71] F. del Aguila, J. A. Aguilar-Saavedra, and R. Pittau, *JHEP* **10**, 047 (2007), [arXiv:hep-ph/0703261 \[hep-ph\]](#).
- [72] K. Huitu, S. Khalil, H. Okada, and S. K. Rai, *Phys. Rev. Lett.* **101**, 181802 (2008), [arXiv:0803.2799 \[hep-ph\]](#).
- [73] A. Atre, T. Han, S. Pascoli, and B. Zhang, *JHEP* **05**, 030 (2009), [arXiv:0901.3589 \[hep-ph\]](#).
- [74] A. Das, P. Konar, and S. Majhi, *JHEP* **06**, 019 (2016), [arXiv:1604.00608 \[hep-ph\]](#).
- [75] R. Ruiz, M. Spannowsky, and P. Waite, (2017), [arXiv:1706.02298 \[hep-ph\]](#).
- [76] A. Abulencia *et al.* (CDF), *Phys. Rev. Lett.* **98**, 221803 (2007), [arXiv:hep-ex/0702051 \[hep-ex\]](#).
- [77] S. Chatrchyan *et al.* (CMS), *Phys. Lett.* **B717**, 109 (2012), [arXiv:1207.6079 \[hep-ex\]](#).
- [78] *Search for Majorana neutrino production in pp collisions at sqrt(s)=7 TeV in dimuon final states with the ATLAS detector*, Tech. Rep. ATLAS-CONF-2012-139 (CERN, Geneva, 2012).
- [79] V. Khachatryan *et al.* (CMS), *Phys. Lett.* **B748**, 144 (2015), [arXiv:1501.05566 \[hep-ex\]](#).
- [80] G. Aad *et al.* (ATLAS), *JHEP* **07**, 162 (2015), [arXiv:1506.06020 \[hep-ex\]](#).
- [81] V. Khachatryan *et al.* (CMS), *JHEP* **04**, 169 (2016), [arXiv:1603.02248 \[hep-ex\]](#).
- [82] F. del Aguila, J. de Blas, and M. Perez-Victoria, *Phys. Rev.* **D78**, 013010 (2008), [arXiv:0803.4008 \[hep-ph\]](#).
- [83] E. Akhmedov, A. Kartavtsev, M. Lindner, L. Michaels, and J. Smirnov, *JHEP* **05**, 081 (2013), [arXiv:1302.1872 \[hep-ph\]](#).
- [84] L. Basso, O. Fischer, and J. J. van der Bij, *Europhys. Lett.* **105**, 11001 (2014), [arXiv:1310.2057 \[hep-ph\]](#).
- [85] S. Antusch and O. Fischer, *JHEP* **10**, 094 (2014), [arXiv:1407.6607 \[hep-ph\]](#).
- [86] M. Aaboud *et al.* (ATLAS), *New J. Phys.* **18**, 093016 (2016), [arXiv:1605.06035 \[hep-ex\]](#).
- [87] A. M. Sirunyan *et al.* (CMS), *JHEP* **07**, 121 (2017), [arXiv:1703.03995 \[hep-ex\]](#).
- [88] G. Aad *et al.* (ATLAS), *JHEP* **06**, 035 (2014), [arXiv:1404.2500 \[hep-ex\]](#).
- [89] M. Aaboud *et al.* (ATLAS), (2017), [arXiv:1706.03731 \[hep-ex\]](#).
- [90] G. Aad *et al.* (ATLAS), *Eur. Phys. J.* **C76**, 259 (2016), [arXiv:1602.09058 \[hep-ex\]](#).
- [91] T. Sjostrand, S. Mrenna, and P. Z. Skands, *JHEP* **05**, 026 (2006), [arXiv:hep-ph/0603175 \[hep-ph\]](#).

- [92] J. de Favereau, C. Delaere, P. Demin, A. Giammanco, V. Lemaître, A. Mertens, and M. Selvaggi (DELPHES 3), *JHEP* **02**, 057 (2014), [arXiv:1307.6346 \[hep-ex\]](#).
- [93] M. Selvaggi, *Proceedings, 15th International Workshop on Advanced Computing and Analysis Techniques in Physics Research (ACAT 2013)*, *J. Phys. Conf. Ser.* **523**, 012033 (2014).
- [94] A. Mertens, *Proceedings, 16th International workshop on Advanced Computing and Analysis Techniques in physics (ACAT 14)*, *J. Phys. Conf. Ser.* **608**, 012045 (2015).
- [95] M. Cacciari, G. P. Salam, and G. Soyez, *JHEP* **04**, 063 (2008), [arXiv:0802.1189 \[hep-ph\]](#).
- [96] M. Cacciari and G. P. Salam, *Phys. Lett.* **B641**, 57 (2006), [arXiv:hep-ph/0512210 \[hep-ph\]](#).
- [97] M. Cacciari, G. P. Salam, and G. Soyez, *Eur. Phys. J.* **C72**, 1896 (2012), [arXiv:1111.6097 \[hep-ph\]](#).
- [98] *Expected performance of the ATLAS b-tagging algorithms in Run-2*, Tech. Rep. ATL-PHYS-PUB-2015-022 (CERN, Geneva, 2015).
- [99] M. Drees, H. Dreiner, D. Schmeier, J. Tattersall, and J. S. Kim, *Comput. Phys. Commun.* **187**, 227 (2015), [arXiv:1312.2591 \[hep-ph\]](#).
- [100] D. Dercks, N. Desai, J. S. Kim, K. Rolbiecki, J. Tattersall, and T. Weber, *Comput. Phys. Commun.* **221**, 383 (2017), [arXiv:1611.09856 \[hep-ph\]](#).
- [101] A. L. Read, *Advanced Statistical Techniques in Particle Physics. Proceedings, Conference, Durham, UK, March 18-22, 2002*, *J. Phys.* **G28**, 2693 (2002), [,11(2002)].